IMPROVED fMRI GROUP STUDIES BASED ON SPATIALLY VARYING NON-PARAMETRIC BOLD SIGNAL MODELING

Philippe Ciuciu[(1,2)]*, Thomas Vincent*[(1,2)]*, Anne-Laure Fouque*[(1,2)] *and Alexis Roche*[(1,2)]

[(1)] CEA, NeuroSpin, Bât. 145, F-91191 Gif-sur-Yvette, cedex France
[(2)] IFR 49, Functional neuroimaging institute, Paris, France
[1] firstname.lastname@cea.fr

ABSTRACT

Multi-subject analysis of functional Magnetic Resonance Imaging (fMRI) data relies on within-subject studies, which are usually conducted using a massively univariate approach. In this paper, we investigate the impact of a novel within-subject analysis on group studies. Our approach is based on the use of spatial mixture models (SMM) in a *joint detection-estimation* framework (JDE) [1]. This setting allows us to characterise the hemodynamic filter at a regional scale and therefore to account for its spatial variability. As the subject-specific BOLD effects enter as input parameters in the computation of group statistics, we then compare two kinds of Random effect analyses (RFX). The first one takes the estimated BOLD effects computed by SPM[1] as inputs while the second one considers the results of our JDE scheme. We finally show on a real dataset of 15 subjects that brain activations appear more spatially resolved using SMM instead of SPM and that a better sensitivity is achieved. Moreover, the JDE framework allows to assess the regional inter-subject variability of the brain dynamics.

***Index Terms*—** RFX analysis, detection-estimation, fMRI.

1. INTRODUCTION

The objective of fMRI group analysis is to extract a good representation of the relationship between brain structure and function across subjects. It usually consists in averaging responses after a normalization procedure that ensures the definition of a common anatomical space for all scanned subjects. Generally, this averaging procedure is implemented using the standard Student-t statistic, and relies on the assumption that the activity is normally distributed across subjects. The fMRI data acquired for each subject during the same cognitive experiment are processed individually to produce an image of estimated BOLD effects relative to a given contrast of experimental conditions. These BOLD effects are usually estimated in the General Linear Model (GLM) framework from the individual data. Classical GLM-based approaches consider a known shape for the impulse response of the neurovascular system (the Hemodynamic Response Function) and assume overall that it is constant throughout the brain.

Recently, a Bayesian detection-estimation approach has been proposed in [2]. This method jointly detects which parts of the brain are activated by a given stimulus type and estimates the underlying dynamics of activations. Further extended in [1], spatial mixture models (SMM) have been introduced to model spatial correlation of fMRI data instead of smoothing them.

This paper is structured as follows. Classical GLM-based inference (SPM) at the subject level is exposed in Section 2 with a special emphasis on how flexible modeling of the BOLD response is achievable in this framework. Our solution presented in Section 3. It relies on a prior parcellation of fMRI data, which is nothing but a clustering procedure that preserves connexity and functional homogeneity. Then, at the parcel level the JDE framework allows us to specify and estimate a specific BOLD model. Section 4 is devoted to group studies in fMRI. The principles of random effect analysis are reminded and a special attention is paid to the permutation test approach. Results obtained at the group level on a quick mapping fMRI experiment are discussed in the fifth and conclusions are drawn in final section.

[1] http://www.fil.ion.ucl.ac.uk/spm

2. WITHIN-SUBJECT ANALYSIS IN fMRI

2.1. Standard GLM-based approach

Within-subject analysis in fMRI is usually addressed using a hypothesis-driven approach that postulates a model of the HRF response and enable local inference at the voxel level. Such methods take place in the General Linear Model (GLM) framework. GLM-based methods correspond to hypothesis-driven approaches that postulate a canonical model for the HRF $\boldsymbol{h}_c$ and enable voxelwise inference. SPM. In its simplest form, the ensuing model of the BOLD response is spatially invariant and remains constant across the brain. Hence, each column or regressor in the *design* matrix $\boldsymbol{X}$ derives from the convolution of $\boldsymbol{h}_c$ with the stimulation signal $\boldsymbol{x}^m$ associated to the m^{th} stimulus type. The GLM therefore reads:

$$[\boldsymbol{y}_1, \ldots, \boldsymbol{y}_J] = \boldsymbol{X}\,[\boldsymbol{\beta}_1, \ldots, \boldsymbol{\beta}_J] + [\boldsymbol{b}_1, \ldots, \boldsymbol{b}_J] \qquad (1)$$

where $\boldsymbol{y}_j$ is the fMRI time series measured in voxel V_j at times $(t_n)_{n=1:N}$ and $\boldsymbol{\beta}_j \in \mathbb{R}^M$ defines the vector of BOLD effects in V_j for all stimulus type $m = 1 : M$. Noise $\boldsymbol{b}_j$ is usually modelled as a first-order autoregressive (*i.e.,* AR(1)) process in order to account for the spatially-varying temporal correlation of fMRI data [3]: $b_{j,t_n} = \rho_j\, b_{j,t_{n-1}} + \varepsilon_{j,t_n}$, $\forall j$, t, with $\boldsymbol{\varepsilon}_j \sim \mathcal{N}(\mathbf{0}_N, \sigma^2_{\varepsilon_j} \boldsymbol{I}_N)$, where $\mathbf{0}_N$ is a null vector of length N, and $\boldsymbol{I}_N$ stands for the identity matrix of size N. Then, the estimated BOLD magnitudes $\widehat{\boldsymbol{\beta}}_j$ in V_j are computed in the maximum likelihood sense by:

$$\widehat{\boldsymbol{\beta}}_j = \underset{\boldsymbol{\beta} \in \mathbb{R}^M}{\arg\min} \|\boldsymbol{y}_j - \boldsymbol{X}\boldsymbol{\beta}_j\|^2_{\widehat{\sigma}^{-2}_{\varepsilon_j}\widehat{\boldsymbol{\Lambda}}_j},$$

where $\widehat{\sigma}^{-2}_{\varepsilon_j}\widehat{\boldsymbol{\Lambda}}_j$ defines the inverse of the estimated autocorrelation matrix of $\boldsymbol{b}_j$; see for instance [4] for details about the identification of the noise structure. Later, extensions that incorporate prior information on the BOLD effects $(\boldsymbol{\beta}_j)_{j=1:J}$ have been developed in the Bayesian framework [5]. In such cases, vectors $(\widehat{\boldsymbol{\beta}}_j)_{j=1:J}$

are computed using more computationally demanding strategies [5]. However, all these GLM-based contributions consider a unique and global model of the HRF shape while intra-individual differences in its characteristics have been exhibited between cortical areas [6].

2.2. Flexible GLM models

Although smaller than inter-individual fluctuations, the within-subject regional variability of the HRF is large enough to be regarded with care. GLM can actually be refined to allow variations of the canonical HRF $\boldsymbol{h}_c$ at the voxel level through additional regressors: $\boldsymbol{h}_c$ can be supplemented with its first and second derivatives ($[\boldsymbol{h}_c \,|\, \boldsymbol{h}'_c \,|\, \boldsymbol{h}''_c]$) to model eg. differences in time-to-peak. Although powerful and elegant, flexibility is achievable at the expense of fewer effective degrees of freedom and decreased sensitivity in any subsequent statistical test. Importantly, in a GLM involving several regressors per condition, the BOLD effect becomes multivariate ($\boldsymbol{\beta}_j^m \in \mathbb{R}^P$) and the Student-t statistic can no longer be used to infer on differences $\boldsymbol{\beta}_j^m$–$\boldsymbol{\beta}_j^n$ between the m^{th} and n^{th} stimulus types. Rather, an *unsigned* Fisher statistic has to be computed, making direct interpretation of activation maps more difficult.

3. BEYOND THE GLM TO WITHIN-SUBJECT ANALYSIS

3.1. Multi-subject parcellation

Here, we claim the necessity of a spatially varying HRF model to keep a *single* regressor per condition, and thus enable direct statistical comparison ($\widehat{\beta}_j^m - \widehat{\beta}_j^n$) feasible. The JDE framework proposed in [1, 2] allows us to introduce a spatially adaptive GLM in which a local estimation of $\boldsymbol{h}$ is performed. To conduct the analysis efficiently, HRF estimation is performed at a regional scale coarser than the voxel level. To define this scale, the functional brain mask is divided in K functionally homogeneous *parcels* using the parcellation technique proposed in [7]. This algorithm relies on the minimisation of a compound criterion reflecting both the spatial and functional structures and hence the topology of the dataset. The spatial similarity measure favours the closeness in the Talairach coordinates system. The functional part of this criterion is computed on parameters that characterise the functional properties of the voxels, for instance the fMRI time series themselves.

The number of parcels K is set by hand. The larger the number of parcels, the higher the degree of within-parcel homogeneity but potentially the lower the signal-to-noise ratio (SNR). To objectively choose an adequate number of parcels, Bayesian information criterion (BIC) and cross validation techniques have been used in [8] on an fMRI study of ten subjects. The authors have shown converging evidence for $K \approx 500$ for a whole brain analysis leading to typical parcel sizes around a few hundreds voxels. Importantly, since the parcellation is derived at the group level, there is a one-to-one correspondance of parcels across subjects, as shown in Fig. 1 .

3.2. Parcel-based modeling of the BOLD signal

Here, we use the parcel-based model of the BOLD signal introduced in [1,2]. As shown in Fig. 2, this means that although the HRF shape $\boldsymbol{h}$ is assumed constant within a parcel, the magnitude of activation β_j^m can vary in space and across stimulus types. Let $\mathcal{P} = (V_j)_{j=1:J}$ be the current parcel. Then, the generative BOLD model reads:

$$\boldsymbol{y}_j = \sum_{m=1}^{M} \beta_j^m \boldsymbol{X}^m \boldsymbol{h} + \boldsymbol{P}\boldsymbol{\ell}_j + \boldsymbol{b}_j, \quad \forall\, j,\ V_j \in \mathcal{P}. \qquad (2)$$

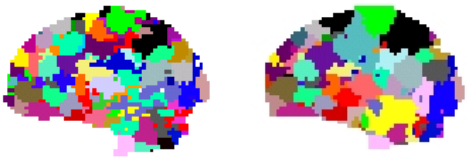

Fig. 1. Sagittal views of a color-coded multi-subject parcellation. Left: Subject 1. Right: Subject 2.

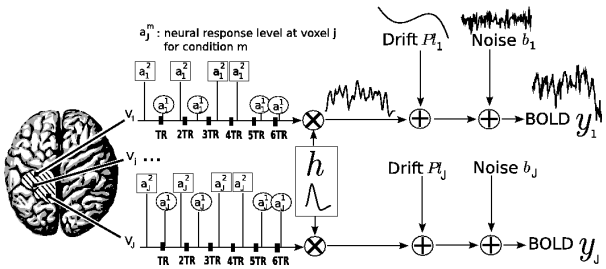

Fig. 2. Regional model of the BOLD signal in the JDE framework. The neural response levels a_j^m match with the BOLD effects β_j^m.

$\boldsymbol{X}^m$ denotes the $N \times (D+1)$ binary matrix that codes the onsets of the m^{th} stimulus. Vector $\boldsymbol{h} \in \mathbb{R}^{D+1}$ represents the unknown HRF shape in $\mathcal{P}$. The term $\boldsymbol{P}\ell_j$ models a low-frequency trend to account for physiological artifacts and noise $\boldsymbol{b}_j \sim \mathcal{N}(\boldsymbol{0}_N, \sigma_{\varepsilon_j}^2 \boldsymbol{\Lambda}_j^{-1})$ stands for the above mentioned AR(1) process.

3.3. Spatial mixture modeling and Bayesian inference

The HRF shape $\boldsymbol{h}$ and the associated BOLD effects $(\boldsymbol{\beta}_j)_{j=1:J}$ are jointly estimated in $\mathcal{P}$. Since no parametric model is considered for $\boldsymbol{h}$, a smoothness constraint on the second order derivative is introduced to regularize its estimation; see [2]. On the other hand, our approach also aims at *detect*ing which voxels in $\mathcal{P}$ elicit activations in response to stimulation. To this end, prior mixture models are introduced on $(\boldsymbol{\beta}^m)_{m=1:M}$ to segregate activating voxels from the non-activating ones in a stimulus-specific manner (*i.e.,* for each m). In [1], it has been shown that SMMs allows us to recover clusters of activation instead of isolated spots and hence to account for spatial correlation in the activation detection process without smoothing the data. As our approach stands in the Bayesian framework, other priors are formulated upon every other sought object in model (2). The reader is referred to [1, 2] for their expressions. Finally, inference is based upon the full posterior distribution $p(\boldsymbol{h}, (\boldsymbol{\beta}_j), (\boldsymbol{\ell}_j), \boldsymbol{\Theta} \,|\, \mathbb{y})$, which is sampled using a Gibbs sampling scheme [1]. Posterior mean (PM) estimates are therefore computed from these samples according to: $\widehat{x}^{\text{PM}} = \sum_{k=L_0}^{L_1} x^{(k)}/L, \quad \forall\, x \in \{\boldsymbol{h}, (\boldsymbol{\beta}_j), \boldsymbol{\Theta}\}$ where $L = L_1 - L_0 + 1$ and L_0 stands for the length of the burn-in period. Note that this estimation process has to be repeated over each parcel of each subject's brain. Since the fMRI data are considered spatially independent across parcels, parallel implementation of the Gibbs sampler implies processing each parcel separately: whole brain analysis is achievable in about 60 mn for $N = 125$ and $K = 500$ and decreases with K. Our current implementation is in `Python` allowing us to take advantage of a parallel computing system available through the `Seppo` library combined with the `Pyro` server. Computation time can be reduced further by using a larger number of processes, for instance to 27 mn for height processes on a dual core quadri processors Pentium IV (2.7 GHz).

4. GROUP ANALYSIS

4.1. Classical parametric population-based inference

Assume S subjects are selected randomly in a population of interest and submitted to the same fMRI experiment. As shown in previous sections, the two types of within-subject analyses produce, in one particular voxel V_j of the standardized space (usually, the MNI/Talairach space) and for each subject s, BOLD effect estimates $\widehat{\boldsymbol{\beta}}_{j,s}$. Comparison between experimental conditions is usually addressed through contrasts *i.e.,* through signed differences $\widehat{d}^{m-n}_{j,s} = \widehat{\beta}^{m}_{j,s} - \widehat{\beta}^{n}_{j,s}$ of the BOLD effects relative to the m^{th} and n^{th} stimulus types. For notational convenience, we will drop index j and the contrast under study $m-n$ in what follows. While the estimated difference $\widehat{d}_s$ generally differs from the true but unobserved effect d_s, assume for now perfect within-subject estimation so that $\widehat{d}_s = d_s$ for $s = 1 : S$. We thus are given a sample $(d_1, , \ldots, d_S)$ drawn from an unknown probability density function (pdf) $f(d)$ that describes the distribution of the effects in the population. Here, we are concerned with inferences about a location parameter (mean, median, mode, ...). Assume for instance we wish to test the null hypothesis that the population mean is negative: $H_0 : \quad \mu_{\text{G}} = \int d\, f(d)\, dd \leq 0$ where $_{\text{G}}$ stands for the group. To that end, we may use the classical one-sample t test and compute the t statistic:

$$t = \frac{\hat{\mu}_{\text{G}}}{\hat{\sigma}_{\text{G}}/\sqrt{S}}, \text{ with : } \hat{\mu}_{\text{G}} = \frac{\sum_s d_s}{S}, \ \hat{\sigma}^2_{\text{G}} = \frac{\sum_s (d_s - \hat{\mu}_{\text{G}})^2}{S-1} \quad (3)$$

Next, we accept the alternative H_1: $\mu_{\text{G}} > 0$, if the probability under H_0 of attaining the observed t value is lower than a given false positive rate. If $f(d)$ is Gaussian, this probability is well-known to be obtained from the Student distribution with $S-1$ degrees of freedom. In this parametric context, the t statistic can be proved to be optimally sensitive (technically, in the sense of the uniformly most powerful unbiased test, see [9]).

4.2. Non-Gaussian populations

If normality is not tenable, however, the Student distribution is valid only in the limit of large samples, and may thus lead to inexact control over the false positive rate in small samples. This problem can be worked around using non-parametric calibration schemes such as sign permutations [9], which allow exact inferences under a milder assumption of symmetry regarding $f(d)$. Although we recommend permutation tests, they only provide an alternative strategy of thresholding a given statistic and, as such, address a *specificity* issue.

The fact that the sampling pdf $f(d)$ may not be normal also raises a *sensitivity* issue as the t statistic may no longer yield optimal power when normality does not hold. Without prior knowledge of the shape of $f(d)$, a reasonable default choice for the test statistic is one that maintains good detection performance over a wide range of pdfs. Such a statistic is robust, not quite in the classical sense of being resistant to outliers, but in the looser sense of being resistant to distributions that tend to produce outliers, such as heavy-tailed, or multimodal distributions.

The sign statistic t_{sgn} is the number of positive values in a sample (using the convention that zero counts half). If the observations are exact, t_{sgn} provides an efficient test of the population median: under the null hypothesis that the median is zero, t_{sgn} follows a binomial law $\mathcal{B}_{S,\frac{1}{2}}$ whatever the shape of f. The Wilcoxon's signed rank (WSR) statistic is a classical alternative to the sign statistic that works by sorting the absolute effects in ascending order,

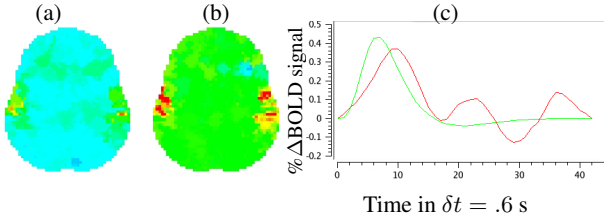

Fig. 3. BOLD effects estimates $(\widehat{d}_j^{\text{A.}-\text{V.}})_j$ in a given subject for the $\text{A.} - \text{V.}$ contrast. **(a)**: SPM-based results obtained with the canonical HRF $\boldsymbol{h}_c$. **(b)**: JDE-based results considering model (2). c: Comparison of HRF shapes in the mostly activated parcel $\mathcal{P}$: $\boldsymbol{h}_c$ and $\widehat{\boldsymbol{h}}_{\mathcal{P}}$ appear in red and , respectively.

then summing up the ranks multiplied by the corresponding effect's signs, yielding: $t_{\text{WSR}} = \sum_{s=1}^{S} \text{sgn}(\widehat{d}_s)\, \text{rank}(|\widehat{d}_s|)$ It is meaningful to interpret WSR statistic as a measure of symmetry about zero. More specifically, if the observations are exact and if the population median is zero, we easily prove that t_{WSR} is S times the non-parametric maximum likelihood estimate of the covariance $\phi(f) = \text{Cov}\big(\text{sgn(D)}, \text{F}_+(|\text{D}|)\big)$ where F_+ is the cumulative distribution function of $|D|$, that is: $F_+(u) = F(u) - F(-u)$ for $u \geq 0$. Clearly, $\phi(f) = 0$ if the effect's sign and the effect's absolute value are statistically independent, a situation that occurs if f is symmetric about zero. In such cases, rejecting $\phi(f) = 0$ implies that the (unique) location parameter of f is different from zero. In the following, we use the WSR statistic as already done in [10].

5. EXPERIMENTAL RESULTS

Real fMRI data were recorded in fifteen volunteers during an experiment, which consisted of a single session of $N = 125$ scans lasting $TR = 2.4$ s each. The main goal of this experiment was to quickly map several brain functions such as motor, visual and auditory responses, as well as higher cognitive functions like computation. Here, we only focus on the auditory and visual experimental conditions and so on the *auditory-visual* contrast of interest (referenced as $\text{A.}-\text{V.}$).

5.1. Within-subject analyses

We compare the BOLD effect estimates for the two within-subject analyses under study. Fig. 3 clearly emphasizes for the $\text{A.}-\text{V.}$ contrast that the JDE method achieves a better sensitivity (bilateral activations) in comparison with GLM-based inference when processing *unsmoothed* data. Indeed, the BOLD effects $\widehat{d}_j^{\text{A.}-\text{V.}}$ have higher values in Fig. 3(b) and appear more enhanced. This is partly due to the modeling of spatial correlation using SMM in the JDE framework. As shown in Fig. 3(c)-[red line], notice that the HRF estimate $\widehat{\boldsymbol{h}}_{\mathcal{P}}$ computed in the mostly activating parcel deviates from the canonical shape depicted in Fig. 3(c)[green line].

5.2. Random effect analyses

To enforce the coherence of our group level comparison with actual pipelines for fMRI data processing (SPM, FSL), the fMRI images that enter in model (1) were spatially filtered using isotropic Gaussian smoothing at 5mm. In the JDE formalism, we still consider unsmoothed but normalized data to build the group parcellation as described in Fig. 4. Note that both approaches will be available in the next release of `BrainVisa` in April, 2008.

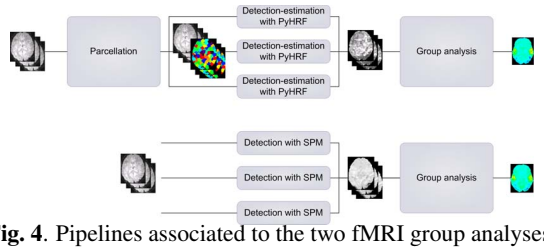

Fig. 4. Pipelines associated to the two fMRI group analyses.

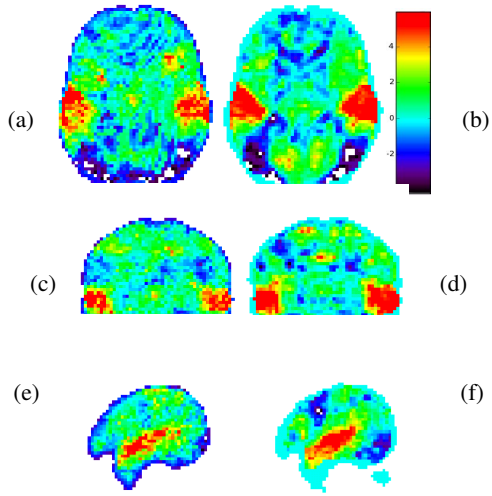

Fig. 5. RFX anaylsis maps based on the WSR statistics in the slice corresponding to the mostly activated cluster. **Radiological** convention: left is right. **(a)-(c)-(e)** and **(b)-(d)-(f)**: results obtained using the JDE and SPM analyses at the subject level, respectively.

Fig. 5 provides us with the WSR statistical maps, corrected for multiple comparisons in the permutation testing framework. The displayed slices match with the place of most significant activations. Activation clusters appear larger in Fig. 5(b-d-f), *i.e.,* using the GLM based approach, as a direct consequence of smoothing. The statistical map derived at the group level from the JDE analyses seems to have a lesser extent while being more significant at the cluster level than the GLM counterpart in the right hemisphere (left side). Moreover, the JDE formalism allows us to detect a gain in sensitivity since activations in Broca's area can be seen in the front of Fig. 5(a), right side. Table 1 confirms quantitatively these results and emphasizes that GLM-based inference systematically reports clusters of larger size (see col. 3). However, in terms of significance, the situation appears more contrasted since cluster level p-value is lower in the right hemisphere for JDE (top line in Table 1) in one cluster over two and thus provides most significant activation. This might be a consequence of the between-subject variability we observed in the HRF estimate as reported in Fig. 6.

Table 1. Suprathreshold clusters summary for the WSR statistic.

	Cluster level p_{corr}	Cluster size (voxels)	Voxel level p_{corr}	Peak coords. x	y	z
JDE	**0.002**	**1151**	$1e-06$	8	30	26
	0.003	876	0.0007	47	27	30
SPM	0.0022	1788	0.0001	5	29	28
	0.0028	**1680**	0.0001	45	27	27

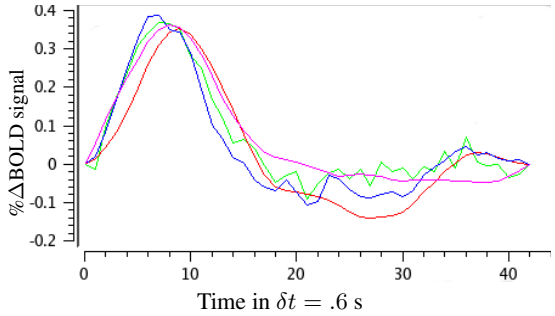

Fig. 6. Subjects are color-coded: HRF estimates computed over the parcel associated to the voxel of maximal WSR value.

6. CONCLUSION

In this paper, we have demonstrated that the statistics computed at the group level are influenced by the type of within-subject fMRI analysis. In particular, we have shown that the JDE formalism is able to provide the neuroscientist with reliable RFX analysis results that can be more sensitive than standard GLM-based inference while avoiding spatial filtering of fMRI images. Finally, we have made the between-subject variability of brain dynamics feasible using non-parametric modeling of the BOLD signal.

7. REFERENCES

[1] T. Vincent, P. Ciuciu, and J. Idier, "Spatial mixture modelling for the joint detection-estimation of brain activity in fMRI," in *32th Proc. ICASSP*, Hawaii, 2007, vol. I, pp. 325–328.

[2] S. Makni, P. Ciuciu, J. Idier, and J.-B. Poline, "Joint detection-estimation of brain activity in fMRI: a multichannel deconvolution solution," *IEEE Trans. Sig. Proc.*, 53, pp. 3488–, 2005.

[3] K.J. Worsley, C.H. Liao, J. Aston, V. Petre, G.H. Duncan, F. Morales, and A.C. Evans, "A general statistical analysis for fMRI data," *Neuroimage*, vol. 15, no. 1, pp. 1–, 2002.

[4] W. D. Penny, S. Kiebel, and K. J. Friston, "Variational Bayesian inference for fMRI time series," *Neuroimage*, vol. 19, pp. 727–, 2003.

[5] M. Woolrich, M. Jenkinson, J. Brady, and S. Smith, "Fully Bayesian spatio-temporal modelling of fMRI data," *IEEE Trans. Med. Imag.*, vol. 23, pp. 213–, 2004.

[6] Daniel A. Handwerker, John M. Ollinger, , and Mark D'Esposito, "Variation of BOLD hemodynamic responses across subjects and brain regions and their effects on statistical analyses," *Neuroimage*, vol. 21, pp. 1639–, 2004.

[7] B. Thirion, G. Flandin, P. Pinel, A. Roche, P. Ciuciu, and J.-B. Poline, "Dealing with the shortcomings of spatial normalization: Multi-subject parcellation of fMRI datasets," *Hum. Brain Mapp.*, vol. 27, pp. 678–, 2006.

[8] B. Thyreau, B. Thirion and J.-B. Poline, "Anatomo-functional description of the brain: a probabilistic approach," in *31th Proc. ICASSP*, Toulouse, France, 2006, pp. 1109–.

[9] Phillip Good, *Permutation, Parametric, and Bootstrap Tests of Hypotheses*, Springer, 3rd edition edition, 2005.

[10] S. Mériaux, A. Roche, B. Thirion, and G. Dehaene-Lambertz, "Robust statistics for nonparametric group analysis in fMRI," in *Proc. 3th Proc. IEEE ISBI*, Arlington, 2006, pp. 936–.